ADVANCED FUNCTIONAL MATERIALS
www.afm-journal.de

Structure and Potential-Dependent Selectivity in Redox-Metallopolymers: Electrochemically Mediated Multicomponent Metal Separations

*Raylin Chen, Jiangyan Feng, Jemin Jeon, Thomas Sheehan, Christian Rüttiger, Markus Gallei, Diwakar Shukla, and Xiao Su**

Electro-responsive functional materials can play a critical role in selective metal recovery and recycling due to the need for molecular differentiation between transition metals in complex mixtures. Redox-active metallopolymers are a promising platform for electrochemical separations, offering versatile structural tuning and fast electron transfer. First, through a judicious selection of polymer structure between a main-chain metallopolymer (polyferrocenylsilane) and a pendant-group metallopolymer (polyvinylferrocene), charge-transfer interactions and binding strength toward competing metal ions are tuned, which as a result, dictate selectivity. For example, almost an order of magnitude increase in separation factor between chromate and meta-vanadate can be achieved, depending on polymer structure. Second, these metallopolymer electrodes exhibit potential-dependent selectivity that can even flip ion preference, based solely on electrical means—indicating a control parameter that is orthogonal to structural modifications. Finally, this work presents a framework for evaluating electrochemical separations in multicomponent ion mixtures and elucidates the underlying charge-transfer mechanisms resulting in molecular selectivity through a combination of spectroscopy and electronic structure calculations. The findings demonstrate the applicability of redox-metallopolymers in tailored electrochemical separations for environmental remediation, value-added metal recovery, waste recycling, and even mining processing.

1. Introduction

Stimuli-responsive polymer materials have been used in a diverse range of applications, including drug delivery, biosensors, microelectromechanical systems, and functional coatings.[1] Recently, electro-responsive metallopolymers have shown superior performance in selective separation processes, including selective capture of heavy metal oxyanions.[2] While there is an increased understanding of the governing electron transfer, ion transport, and solvation processes within redox-polymers,[3] there remains untapped potential in leveraging these redox-materials for advanced electrochemical separations—especially in the tailoring of structure and electric potential for multicomponent metal recovery from complex mixtures.

Separation and recovery of metal ions from water is vital toward achieving sustainable metal recovery and cleaning up environmental pollution.[4] Capture of metals from industrial and mining wastewaters is critical not only for environmental management, but also for recovery and recycling. Industrial and mining streams often contain multiple valuable metals in multicomponent mixtures, in the presence of competing electrolyte, organic compounds, and other hazardous materials.[5] Thus, these separations are challenging due to their "needle-in-the-haystack" nature, in which target metal ions are present in trace amounts within complex matrices.[4a] There has been extensive work on the recovery of specific metal ions using chemical adsorbents.[6] However, conventional adsorption often requires additional chemicals to regenerate the adsorbent for reuse, thus contributing to waste footprint.[7]

Electroseparations based on redox-active, charge-transfer materials have shown significant promise as a platform for metal ion removal, with specific chemical tuning of adsorption sites enabling high ion-capacity and ion-selectivity.[2b,8] Electrosorption-based approaches for metal recovery can overcome drawbacks of conventional adsorption, as potential-dependent reversibility can eliminate the use of regeneration

R. Chen, J. Feng, J. Jeon, T. Sheehan, Prof. D. Shukla, Prof. X. Su
Department of Chemical and Biomolecular Engineering
University of Illinois
Urbana, Champaign, IL 61820, USA
E-mail: x2su@illinois.edu
Dr. C. Rüttiger
Ernst-Berl-Institute for Chemical Engineering
and Macromolecular Science
Technical University of Darmstadt
Alarich-Weiss Str. 4, Darmstadt D-64287, Germany
Prof. M. Gallei
Chair in Polymer Chemistry
Saarland University
Saarbrücken 66123, Germany
The ORCID identification number(s) for the author(s) of this article can be found under https://doi.org/10.1002/adfm.202009307.

DOI: 10.1002/adfm.202009307

chemicals, and improve adsorption kinetics by promoting counter-ion migration. However, within electrochemical separations, there has been limited work investigating competing ion selectivity. Furthermore, there is a pressing need for the systematic design of electro-responsive systems for multicomponent separations, especially between transition metal ions with similar size and chemical properties. Thus, within the current work, we seek to overcome intrinsic challenges in metal differentiation, by exploring redox-active metallopolymers for multicomponent metal recovery.

We investigate the metal ion selectivity of a pendant-group redox-active polymer, polyvinylferrocene (PVF), and a main-chain polymer, polyferrocenylsilane (PFS), and elucidate the effect of the electron-donating silane group on the ferrocene-binding sites. PVF undergoes a single-electron oxidation, and has shown remarkable activity toward transition metal oxyanion capture for chromium and arsenic.[2a,9] The ion exchange behavior of PVF-films has been extensively studied, including understanding of the nature of the counter-ion on ion-transport and charge-trapping.[3b,c,10] PVF-based materials have ferrocenyl groups on the side-chains, leading to robust single-electron redox-active.[11] In contrast, PFS undergoes a two-electron oxidation due to ferrocene–ferrocene (Fc–Fc) interactions between adjacent Fc's in the main-chain, and displays unique semiconducting properties.[12] PFS homopolymers and block copolymers have been used widely for the self-assembly of highly structured nanostructures.[13] Despite its interesting properties, PFS has not been previously explored for metal ion separations. The distinct properties of PVF and PFS can shed mechanistic insights into structural and electrochemical factors dictating selectivity in electrosorption.

Here, we explore the electrochemical selectivity between PVF and PFS for a series of valuable transition metal oxyanions, targeting broad applications in resource recovery and environmental remediation. The transition metals included in this study are arsenic, chromium, selenium, molybdenum, rhenium, and vanadium. Arsenic is a toxic metalloid that threatens millions of people around the world,[14] used in optical materials and semiconductors (e.g., GaAs).[15] Chromium is also toxic[16] and used to make stainless steels. Selenium is an essential micronutrient but toxic when ingested in large amounts,[17] and often used in metallurgy, as well as pigments.[15] Molybdenum can often be found as a byproduct from copper mining, and used in metallurgical applications.[15] Rhenium can be recovered as a byproduct from roasting molybdenum concentrates, and found in alloys for crucibles, electrical contacts, among other materials.[15] In addition, ReO_4^- has been used as an analogue molecule for TcO_4^-,[18] with Technetium being a radioactive element of interest itself. ^{99m}Tc is used for medical diagnostic procedures and produced through radioactive decay of ^{99}Mo. Thus, selective capture of TcO_4^- is important both to isolate TcO_4^- from MoO_4^{2-} for radionuclide manufacturing, and to treat radioactive Tc waste.[19] Vanadium is both a toxic heavy metal,[20] often used in alloying steels,[15] and also a critical element used in redox flow batteries.[21] Finally, these metals can be commonly found in multicomponent mixtures with inorganic anions, and potentially each other, depending on the industrial wastewater or mining source.

Through a combination of spectroscopy, separation tests, and electronic structure calculations, our work elucidates the structural effect of each distinct metallopolymer structure (pendant-group redox-polymer vs main-chain polymer) on charge-transfer interactions and demonstrates tunable selectivity for specific transition metal oxyanions. We observe that these polymers display selectivity dependency on electric potential, presenting a novel strategy for selectivity control that is orthogonal to the selectivity that arises from polymer structure, thus opening new avenues for advanced materials recycling.

2. Results and Discussion

Nanostructured PVF/carbon nanotube (PVF-CNT) and PFS (specifically polyferrocenyldimethylsilane)/carbon nanotube (PFS-CNT) composite electrodes were prepared using a solution coating method,[22] with PFS synthesis details given in the Experimental Section and Supporting Information. Unlike PVF, which displays cyclic voltammograms with a single oxidation wave (**Figure 1**a,c), PFS displays cyclic voltammograms with two oxidation waves, indicative of a two-step oxidation process due to adjacent Fc–Fc interactions in the main-chain (Figure 1b,d, and Figure S3.6, Supporting Information). High-resolution scanning electron microscopy showed that the PVF-CNT and PFS-CNT thin films had uniform and nanoporous features (Figure 1e,f). Energy-dispersive X-ray spectroscopy (EDS) confirmed the presence of the iron in both metallopolymers-coated electrodes (Figure 1e,f).

The affinity of PFS-CNT to transition metals was first evaluated in electrosorption experiments containing 1 mM of a metal oxyanion sodium salt (Na_2HAsO_4, Na_2MoO_4, or $NaVO_3$) and 20 mM sodium perchlorate supporting electrolyte. Under chronoamperometric conditions, PFS-CNT showed rapid uptake kinetics, reaching equilibrium within 20 min for all oxyanions tested (**Figure 2**b). PFS-CNT achieved uptakes of 65.7 mg g^{-1} As at 1.0 V versus Ag/AgCl, 30.8 mg g^{-1} V at 0.8 V versus Ag/AgCl, and 19.1 mg g^{-1} Mo at 0.8 V versus Ag/AgCl, demonstrating that PFS-CNT can successfully capture these oxyanions in the presence of excess competing perchlorate anions. Even in the absence of supporting electrolyte, PVF-CNT and PFS-CNT still display comparable kinetics with 1 mM of transition metal oxyanion in solution, achieving equilibrium uptake within 20 min (Figure S4.9, Supporting Information)—which confirms applicability of these redox-systems even for metal recovery in low-salinity systems.

Arsenate was taken first as a model oxyanion for electrode performance due to its importance for environmental remediation, and prior studies regarding its electrosorption performance.[2a,23] At tested potentials between 0 and 1.0 V versus Ag/AgCl, PVF-CNT and PFS-CNT displayed similar uptake capacities of arsenate, with both PVF-CNT and PFS-CNT achieving a maximum capacity of approximately 60 mg g^{-1} As at potentials higher than 0.6 V versus Ag/AgCl (Figure 2c). The electrosorption of arsenate was verified with X-ray photoelectron spectroscopy (XPS), showing a clear peak for arsenic on the electrode after adsorption which was absent in the spectra for the unused electrode (Figure 2e). Fe 2p XPS of PFS-CNT after electrosorption agrees that uptake reaches a maximum at 0.6 V

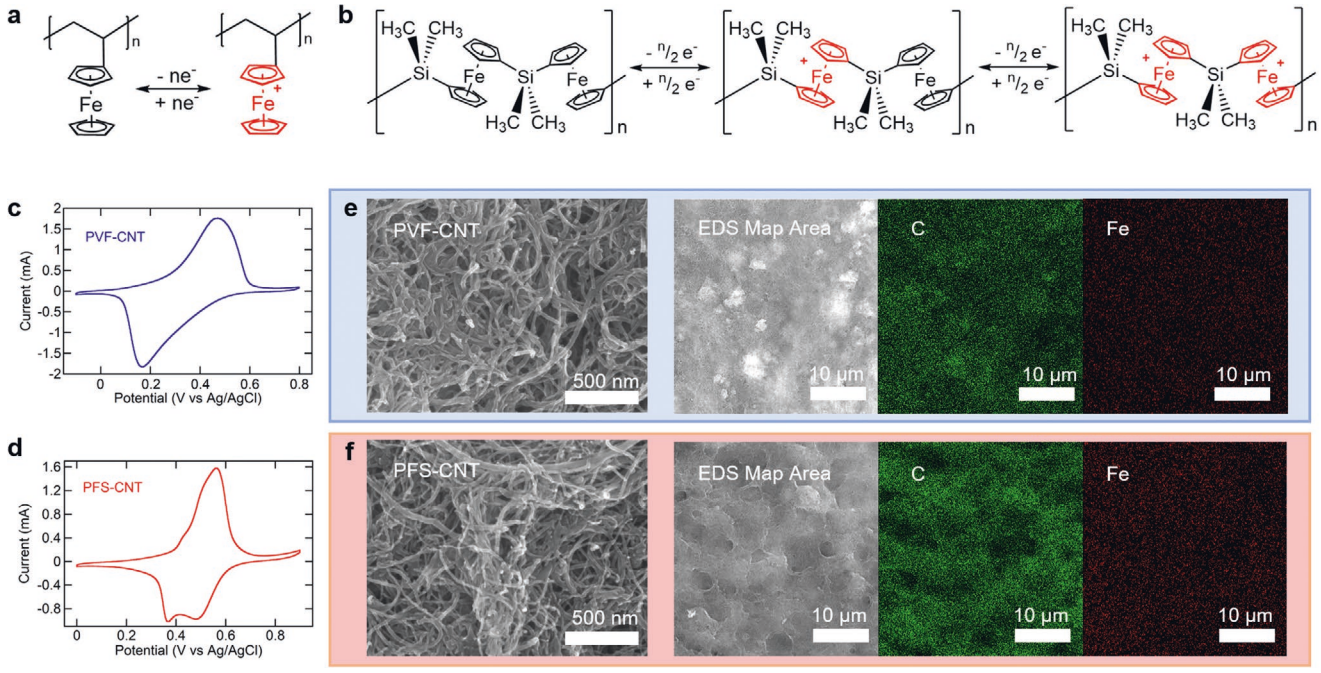

Figure 1. Ferrocene polymer redox and electrode micrographs: a) PVF redox-reaction; b) PFS redox-reaction; c) Cyclic voltammogram of PVF-CNT, 5 mV s^{-1} scan rate in 100 mM $NaClO_4$, purged with N_2; d) Cyclic voltammogram of PFS-CNT, 5 mV s^{-1} scan rate in 100 mM $NaClO_4$, purged with N_2. e) High-resolution SEM and EDS mapping of PVF-CNT electrodes. f) High-resolution SEM and EDS mapping of PFS-CNT electrodes.

Ag/AgCl. The Fe 2p region displays strong spin-orbit splitting with Fe 2p binding energies of 707.8 and 720.6 eV for the $2p_{3/2}$ and $2p_{1/2}$ transitions, respectively, for unoxidized Fc (referenced to C–C C 1s at 284.8 eV).[24] When oxidized to Fc^+, these binding energies shift upward in binding energy to 711.6 and 725.4 eV for the $2p_{3/2}$ and $2p_{1/2}$ transitions, respectively (Figure 2d), and these values are consistent with previously reported Fc^+ binding energies.[25] At 0.4 V, a significant degree of Fc is still unoxidized, as shown by the peaks at 707.8 and 720.6 eV. At 0.6 V and above, the peaks at 707.8 and 720.6 eV disappear with only the peaks corresponding to Fc^+ (711.6 and 725.4 eV) remaining, suggesting that most of the Fc sites have been oxidized at 0.6 V and may explain why raising the potential above 0.6 V did not significantly increase the uptake capacity of PFS-CNT. Based on XPS survey quantification, arsenate and perchlorate were present on the surface in a ratio of 0.81 As:1 Cl (Figure S2.5, Supporting Information). This ratio is much higher than the initial ratio of arsenate to perchlorate in solution (1 As:20 Cl) and indicates that PFS, like PVF,[2a] can also selectively target arsenate in perchlorate-containing solution.

Upon application of a reducing potential, Fc^+ can be reduced back to Fc, and the bound anion is expelled. A series of release conditions were tested with arsenate from 0.0 to –0.4 V versus Ag/AgCl with both PVF-CNT and PFS-CNT (Figure 2f). After electrosorption was performed in a solution containing 1 mM arsenate and 20 mM perchlorate, a reducing potential was applied, and anions were expelled into the same solution that was used to test electrosorption. PVF-CNT showed better release, regenerating up to 70.5% of the captured arsenic upon application of –0.4 V versus Ag/AgCl after 1 h. Maximum release of arsenate from PFS-CNT was 47.5% at –0.2 V versus Ag/AgCl. The incomplete release of arsenate is likely due to the incomplete reduction of PVF-CNT and PFS-CNT (Figure S2.11, Supporting Information). In addition, the lesser release of arsenate from PFS-CNT than from PVF-CNT appears to be due to PFS-CNT having difficulty reducing Fc^+ back to Fc. As measured via XPS, 2.4% of the Fc^+ was reduced at 0.0 V versus Ag/AgCl and 2.5% was reduced at –0.4 V in PFS-CNT. In contrast, for PVF-CNT, 86% of the Fc^+ was reduced at 0.0 V versus Ag/AgCl and 84% of the Fc^+ was reduced at –0.4 V (Figure S2.11, Supporting Information). Shorter cycle times between 0.8 V oxidation and –0.4 V reduction seemed to improve the Fc^+ reduction in PFS-CNT (Figure S2.12, Supporting Information). Following a cycle of 0.8 V for 20 min and –0.4 V for 40 min, 32% of PFS-CNT was in a reduced state. When this cycle was shortened to 0.8 V for 1 min and –0.4 V for 2 min, 57% of PFS-CNT was in a reduced state, as measured by XPS. Recent work suggested that reactive oxygen species could potentially oxidize ferrocene-containing systems under continued use,[26] and thus could hamper Fc^+ reduction. PFS in particular has shown a higher sensitivity to secondary reactions when oxidized.[27] Thus, we expect that further chemical modifications and operation-parameter screening under both aerobic and anaerobic conditions are required to provide insights on enhancing regeneration in the future.

When electrochemically releasing into a clean solution without any electrolyte, PVF-CNT showed comparable release behavior, releasing 62.8%, while PFS-CNT was able to release 96% of the bound arsenic (Figure S4.10, Supporting Information). PVF-CNT and PFS-CNT release kinetics were typically slower than adsorption kinetics, requiring up to 2 h to fully release bound oxyanions depending on the transition metal (Figure S4.10, Supporting Information). The slower release kinetics relative to adsorption has been observed before using

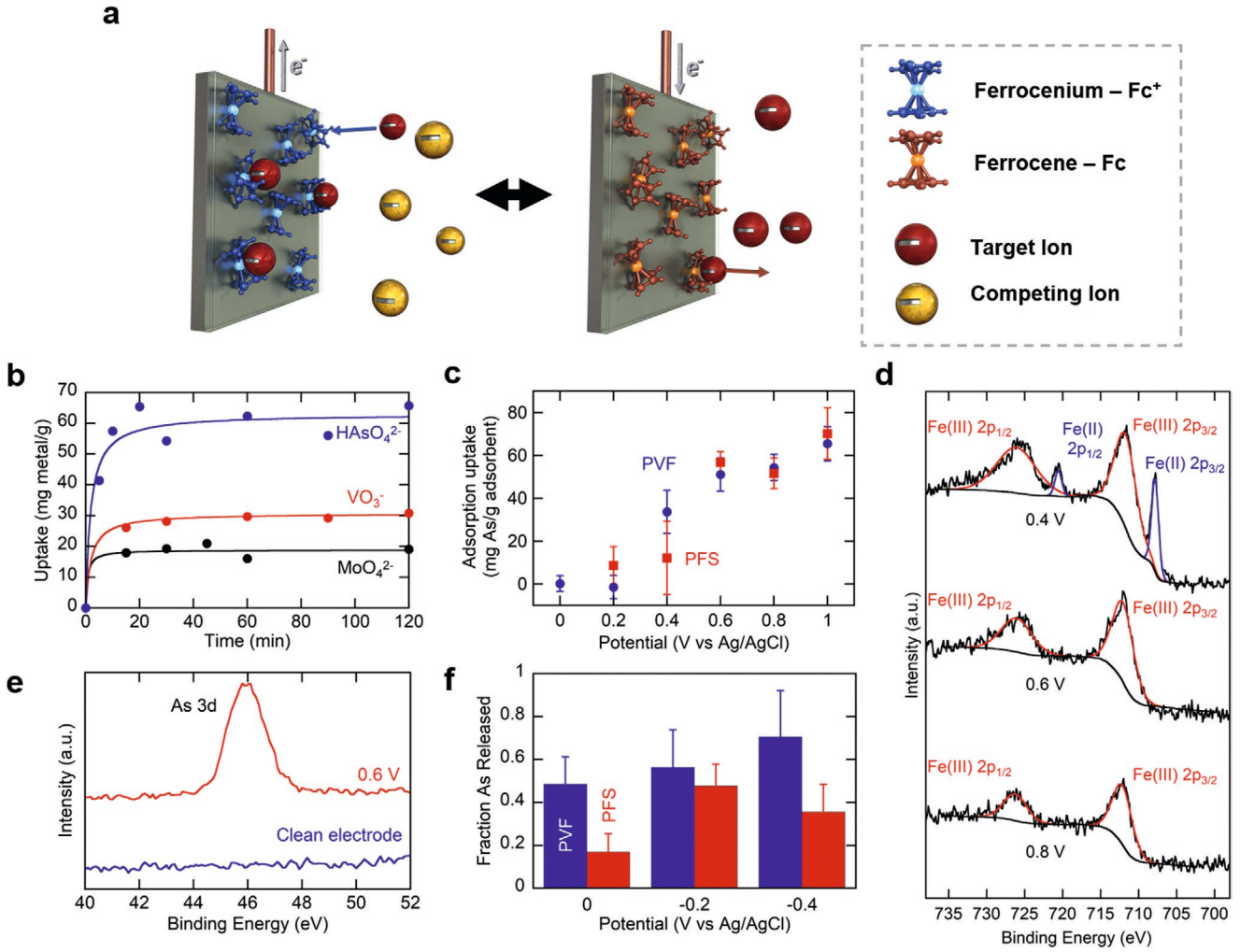

Figure 2. PFS-CNT and PVF-CNT electrosorption with supporting electrolyte. a) Schematic of ferrocene polymer electrosorption and release. Oxidation of ferrocene units to ferrocenium induces selective electrosorption of anions. Reduction of ferrocenium to ferrocene releases the bound anions. b) Adsorption kinetics for various anions using PFS-CNT. Adsorption was carried out at 1.0 V versus Ag/AgCl for $HAsO_4^{2-}$ and 0.8 V versus Ag/AgCl for VO_3^- and MoO_4^{2-} using 1 mM of the oxyanion sodium salt and 20 mM sodium perchlorate supporting electrolyte. c) Equilibrium uptake of As using 1 mM Na_2HAsO_4 and 20 mM sodium perchlorate supporting electrolyte for PVF-CNT and PFS-CNT at various potentials. Data expressed as mean ± standard error of eight ICP-OES measurements. Data for PFS at 0.4, 0.6, and 0.8 V are expressed as mean ± standard deviation of $n = 2$, 4, and 6 replicates, respectively. d) High-resolution Fe 2p XPS OF PFS-CNT after $HAsO_4^{2-}$ electrosorption at various potentials. e) High-resolution As 3d XPS of PFS-CNT before use (as prepared) and after electrosorption of $HAsO_4^{2-}$ at 0.6 V versus Ag/AgCl. f) Fraction of $HAsO_4^{2-}$ released at various applied potentials after 1 h. Data expressed as mean ± standard error of eight ICP-OES measurements.

in situ TEM studies with PVF-films on gold for chromate adsorption.[2a] While adsorption can be fast due to enhanced electrostatics between oxyanions and the ferrocenium cation moiety, oxyanion release from a reduced redox-polymer is mostly entropic and thus much slower.

2.1. Structure-Dependent Selectivity

The selectivity of PVF-CNT and PFS-CNT was screened for the six heavy metal anions ($HAsO_4^{2-}$, CrO_4^{2-}, SeO_4^{2-}, MoO_4^{2-}, VO_3^-, and ReO_4^-) in binary competitive adsorption tests. PVF-CNT or PFS-CNT was immersed in a solution containing 1 mM of two oxyanion sodium salts (2 mM total, e.g., 1 mM Na_2MoO_4 and 1 mM Na_2CrO_4), and electrosorption was induced at various potentials. Selectivity was measured using a separation factor, defined between two species (A and B) to be:

$$\alpha_{A,B} = \frac{N_{A,ads} / N_{B,ads}}{N_{A,sol} / N_{B,sol}} \quad (1)$$

where the $N_{A,ads}$ is the molar quantity of A adsorbed onto the electrode, $N_{B,ads}$ is the molar quantity of B adsorbed onto the electrode, $N_{A,sol}$ is the molar quantity of A remaining in solution, and $N_{B,sol}$ is the molar quantity of B remaining in solution. Separation factors greater than 1 indicate higher selectivity for A as compared to B, while separation factors less than 1 indicate higher selectivity for B as compared to A.

Figure 3a,b shows binary ion-selectivity heat maps for the separation factors obtained using PVF-CNT and PFS-CNT at

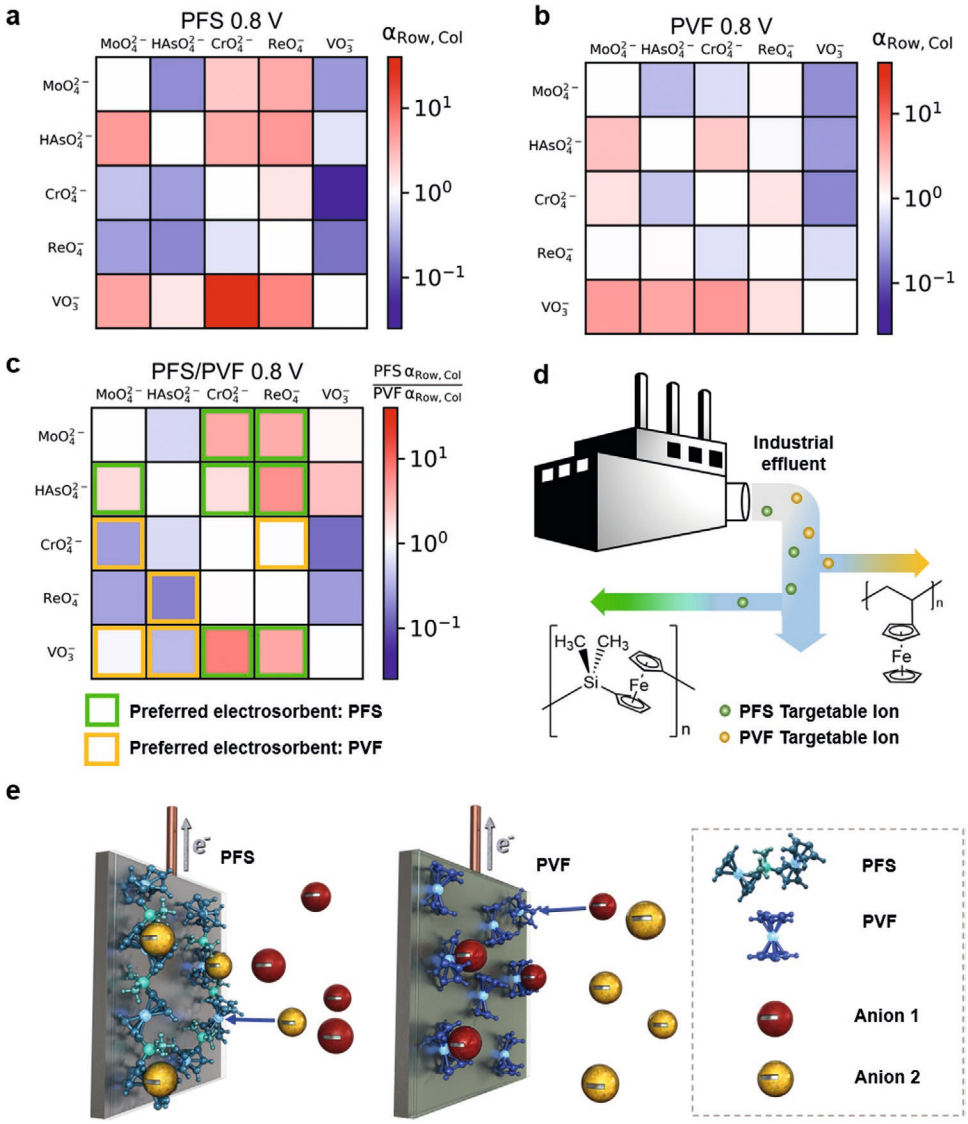

Figure 3. Two component separation factors for PVF-CNT and PFS-CNT—Structural control of selectivity. a) Heat map of separation factors obtained using PFS-CNT for every pair of oxyanions (1 mM each) at 0.8 V Ag/AgCl. b) Heat map of separation factors obtained using PVF-CNT for every pair of oxyanions (1 mM each) at 0.8 V versus Ag/AgCl. c) Heat map of PFS-CNT separation factors divided by PVF-CNT separation factors. PFS had a higher separation factor than PVF in tiles colored red. Green boxes correspond to PFS having a separation factor greater than 1, and PFS had a higher separation factor than PVF (PFS more advantageous than PVF). Tiles highlighted with a yellow box correspond to separations where PVF had a separation factor greater than 1 and PVF had a higher separation factor than PFS. d) Schematic of PFS and PVF being implemented in a metal recovery process. e) Due to differences in selectivity, PFS and PVF can be used to target different ions.

0.8 V versus Ag/AgCl with the anion labeled for each row as species A and the anion labeled for each column as species B in $\alpha_{A,B}$. The goal was to construct a comparative performance map, which can guide polymer selection in multicomponent separations when multiple metals are present within the same mixture. Figure 3c shows the separation factor ratios obtained for PFS-CNT compared to those obtained for PVF-CNT. Boxes highlighted with a green square mark separations where PFS-CNT would yield higher selectivity than PVF-CNT for the specific recovery of the row anion over the column anion. The criteria for higher selectivity is that the separation factor of PFS-CNT for the particular ion combination is higher than that of PVF-CNT, and at the same time, the PFS-CNT separation factor is greater than 1 for that particular binary separation. Boxes highlighted with a yellow square mark separations where PVF-CNT would yield higher selectivity for recovery of the row anion. Due to these differences in selectivity performance, we envision the ability to tailor polymer structures for targeted metal recovery processes, depending on the stream compositions (Figure 3d,e).

In 8 of the 10 binary adsorption tests at 0.8 V versus Ag/AgCl, PVF and PFS favored the same anion. For example, $\alpha_{VO3-,CrO42-}$ was 5.2 for PVF-CNT and 39 for PFS-CNT, indicating VO_3^- had a greater affinity toward PVF-CNT and PFS-CNT than CrO_4^{2-}, but PFS was almost an order of magnitude more selective. In the remaining two binary adsorption tests (MoO_4^{2-} + CrO_4^{2-}, $HAsO_4^{2-}$ + ReO_4^-), PVF-CNT and PFS-CNT

favored different ions ($\alpha_{MoO42-,CrO42-}$ = 0.60 and $\alpha_{HAsO42-,ReO4-}$ = 0.91 for PVF-CNT, $\alpha_{MoO42-,CrO42-}$ = 2.4 and $\alpha_{HAsO42-,ReO4-}$ = 5.2 for PFS-CNT), demonstrating that a change in structure from a pendant ferrocene polymer to a main-chain ferrocene polymer can alter the ion-selectivity trend and furthermore, demonstrating that redox-active polymers can be structurally tuned for targeted ion selectivity. SeO_4^{2-} was omitted from the heat maps because SeO_4^{2-} removal was not significant and resulted in separation factors toward infinity and its inclusion would suppress the colors of other heat map elements (Figure S4.8, Supporting Information). SeO_4^{2-} adsorption and removal has been noted to be especially difficult due to its lack of affinity to conventional adsorbents.[28] Even adsorbents that strongly adsorb selenite ions (SeO_3^{2-}) often cannot effectively adsorb SeO_4^{2-}.[29] It has been noted that selenite ions adsorb strongly by forming inner-sphere complexes while the SeO_4^{2-} anions adsorb by forming outer-sphere complexes.[30] The lack of affinity of the metallopolymers to capture SeO_4^{2-} may suggest that ferrocene is unlikely to directly ligate or form outer-sphere complexes with SeO_4^{2-}. Further chemical design may be needed to create efficient SeO_4^{2-}-specific electrosorbents.

So far, PVF-CNT and PFS-CNT selectivity has only been tested under idealized conditions, where the transition metals are the only oxyanions present and at relatively high concentrations. However, as previously mentioned, real metal ion recovery processes often require targeted ion recovery amidst an abundance of competing ions. To test their practical applicability in a realistic matrix, PVF-CNT and PFS-CNT were tested in real secondary effluent wastewater collected from Urbana-Champaign Sanity District spiked with 1 mg L^{-1} Mo (as Na_2MoO_4) and 1 mg L^{-1} Cr (as Na_2CrO_4); concentrations which are typical of Mo and Cr rich mining streams.[31] At 0.8 V in the spiked wastewater, PFS-CNT and PVF-CNT demonstrate the same ion preference as in the idealized separation factor experiments, with $\alpha_{MoO42-,CrO42-}$ = 1.06 for PFS-CNT and $\alpha_{MoO42-,CrO42-}$ = 0.59 for PVF-CNT (vs 2.4 and 0.60, respectively, in idealized separation factor experiments) demonstrating that the previously observed differential selectivity was preserved in a real, complex matrix (Figure S4.11, Supporting Information). From 1 mL of spiked wastewater, PVF-CNT removed 57% of the Mo and 69% of the Cr, and PFS-CNT removed 29% of the Mo and 27% of the Cr.

Quantum mechanical calculations were performed to elucidate the mechanism of binding. Fc^+ and $FcSi(CH_3)_3^+$ were used to study the effect of an electron donating trimethyl–silane substituent on anion-binding behavior (**Figure 4**a,b, and Figure S6.1, Supporting Information). Calculated binding energies (ΔG) to Fc^+ and $FcSiCH_3)_3^+$ for all six anions are shown in Figure 4c,d. The binding energy to $FcSi(CH_3)_3^+$ was lower than to Fc^+ for all six anions (e.g., 9.87 kcal mol^{-1} for $[Fc–MoO_4]^-$, 7.96 kcal mol^{-1} for $[FcSi(CH_3)_3–MoO_4]^-$) (Figure 4c,d). The lower binding energies to $FcSi(CH_3)_3^+$ are likely due to the electron donating properties of the silane group, which pushes electron density onto the ferrocene and delocalizes its positive charge. Within equivalent structures of [Fc–Anion] and $[FcSi(CH_3)_3–Anion]$, the iron has a much greater positive charge in the former structure (e.g., 0.184 e in $[Fc–MoO_4]^-$ and 0.118 e in $[FcSi(CH_3)_3–MoO_4]^-$) (Table S6.1, Supporting Information). In the $[FcSi(CH_3)_3–Anion]$ structures, much of the positive charge was predicted to be located on the silicon atom (0.406 e in $[FcSi(CH_3)_3–MoO_4]^-$) and as a result, the methyl groups on the silane participated in the binding to anions (Figure 4b). While all tested anion binding energies to $FcSi(CH_3)_3^+$ were lower than to Fc^+, the binding energies shifted by different amounts, which would result in differing anion selectivities between $FcSi(CH_3)_3^+$ and Fc^+.

There appeared to be a negative correlation between the ionization energy of the anion (the energy required to remove an electron from the anion) and the difference in binding energy between that anion and Fc^+ and $FcSi(CH_3)_3^+$ (Figure 4e). We hypothesize that a charge-transfer binding mechanism may be dictating this correlation.[2a] Anions with a low ionization energy may be more willing to give up electron density to the cationic binding site, and as such, the electronegativity of the binding site strongly affects the binding energy and subsequent selectivity. In contrast, anions with a high ionization energy may be unwilling to give up electron density and, therefore, would be agnostic to the identity of the binding site. Instead, the binding energy of anions with high ionization energies may be primarily the electrostatic reward of bringing two oppositely charged ions together. The charge-transfer modulation shown by the addition of the silane substituent demonstrates the opportunity for tunable ferrocene polymers with specific substituents for highly targeted ion capture.

It must be noted that while quantum mechanical calculations are powerful to elucidate atomistic binding and charge-transfer mechanisms, they do not account for more macroscopic phenomenon that may affect the ability of the electrodes to capture ions. For example, previous electrosorption work has shown that variables such as pore size, ion size, and hydrated ion size play a role in how ions can adsorb to porous charged electrodes.[32] VO_3^-, despite having relatively low calculated binding energies (5.44 kcal mol^{-1} with $FcSi(CH_3)_3^+$ and 8.11 kcal mol^{-1} with Fc^+), showed the greatest overall affinity for both PVF-CNT and PFS-CNT as $\alpha_{VO3-,B} > 1$ for all anions B and all potentials except $\alpha_{VO3-,ReO4-}$ at 0.6 V versus Ag/AgCl. This may be because VO_3^- forms polyanion chains of $[VO_3]_n^{n-}$ ($n > 1$).[33] Attachment of one VO_3^- to the electrode could include additional VO_3^- units in a chain, and allow even over-stoichiometric VO_3^- adsorption relative to Fc sites.

2.2. Potential-Dependent Selectivity

The selectivity of PFS-CNT and PVF-CNT changes depending on the applied potential (**Figure 5**, and Figure S4.3–5, Supporting Information). Figure 5a,b highlights two special cases where ion preference switched for the ferrocene polymers at different potentials. $\alpha_{MoO42-,CrO42-}$ at an applied potential of 0.5 V versus Ag/AgCl was 0.28 and 0.43 for PVF-CNT and PFS-CNT, respectively, with more CrO_4^{2-} adsorbed than MoO_4^{2-}. At 1.0 V versus Ag/AgCl, more MoO_4^{2-} was adsorbed and $\alpha_{MoO42-,CrO42-}$was 1.5 and 4.6 for PVF-CNT and PFS-CNT, respectively. A similar swap occurred between ReO_4^- and MoO_4^{2-}, with $\alpha_{MoO42-,ReO4-}$ changing from 0.17 for PVF-CNT and 0.48 for PFS-CNT at 0.5 V Ag/AgCl to 1.8 for PVF and 35 for PFS at 1.0 V versus Ag/AgCl. Tracking the anion speciation as a function of pH and applied potential on Pourbaix diagrams, it seems unlikely that the potential-dependent selectivity is a result of changing anion speciation (Figure S5.4,5,

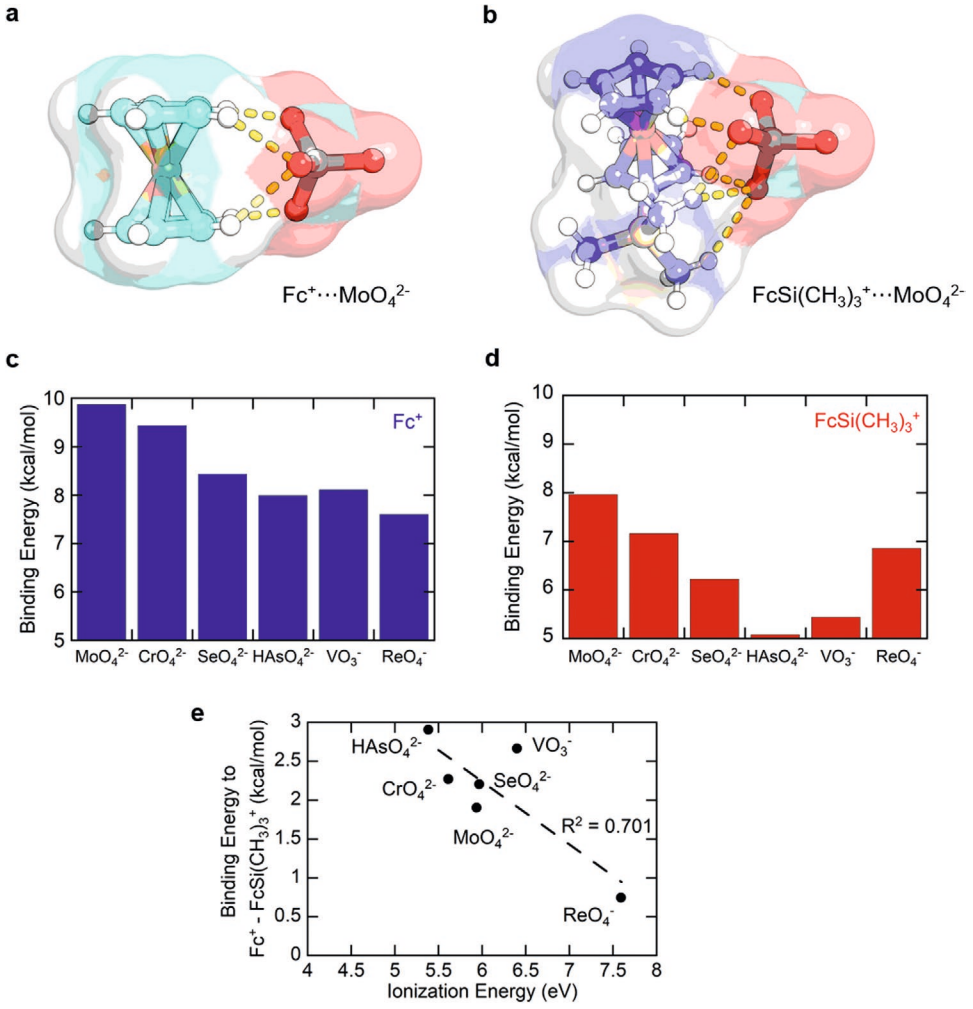

Figure 4. Quantum mechanical calculations. a) Optimized structure of $[Fc–MoO_4]^-$. Labeled distances in units of Å. b) Optimized structure of $[FcSi(CH_3)_3–MoO_4]^-$. Labeled distances in units of Å. c) Binding energetic reward (ΔG) to Fc^+ for the six anions tested, corrected for solvation (implicit) and non-zero temperature. d) Binding energetic reward (ΔG) to $FcSi(CH_3)_3^+$ for the six anions tested, corrected for solvation (implicit) and non-zero temperature. e) Ionization energy versus the difference in binding energy to Fc^+ and $FcSi(CH_3)_3^+$ for the six anions tested. Linear least-squares regression shown by dotted line.

Supporting Information). To support this, there is an absence of anion redox activity on the electrode between different applied potentials, as detected by XPS (Figure 5c–f, and Figure S2.6–9, Supporting Information). The Mo $3d_{5/2}$ peak at 232.9 eV confirms the oxidation state of MoO_4^{2-} at all tested potentials while the Cr $2p_{3/2}$ peak at 577.2 eV suggests CrO_4^{2-} has reduced to a Cr(III) species (likely between the experiment and characterization since CrO_4^{2-} is a strong oxidizing agent) (Figure 5c–f).[34]

A combination of electrostatics and charge-transfer may contribute to the potential-dependent selectivity, in addition to other microscopic pore/solvation effects. We observed that when comparing the separation factors at 0.6 and 1.0 V versus Ag/AgCl, the separation factor shifts in favor of the anion that transfers more charge, an effect seen in 16 out of the 20 anion pair tests at 1.0 V versus Ag/AgCl. That is, $\alpha_{A,B}$, with anion A transferring more charge than anion B, increased when increasing potential from 0.6 to 1.0 V for 16 out of the 20 anion pair tests (10 anion pairs, PVF-CNT and PFS-CNT) (Figures S4.3–5 and S6.2,3, Supporting Information). We hypothesize that this may be the result of a driving force toward satisfying charge neutrality at a microscopic level. As the potential of the electrode increases, the charge density on the surface of the electrode also increases and ions that transfer more charge to the electrode surface may begin to outcompete ions that transfer less charge by better satisfying microscopic charge neutrality. A swapping of ion preference ($\alpha_{A,B}$ crossing 1) was not observed for all anion pairs, however, these results correlate with prior observations that electrode charge density can impact ion-preference at different potentials.[32a,35]

However, other mechanisms for potential-dependent selectivity possibly play a role, due to the complex nature of the electrode–solution interface, so further studies into this correlation are warranted. Previous electrosorption work has shown that the effect of surface change density on the preference of ions adsorbed to that surface is dependent on several factors

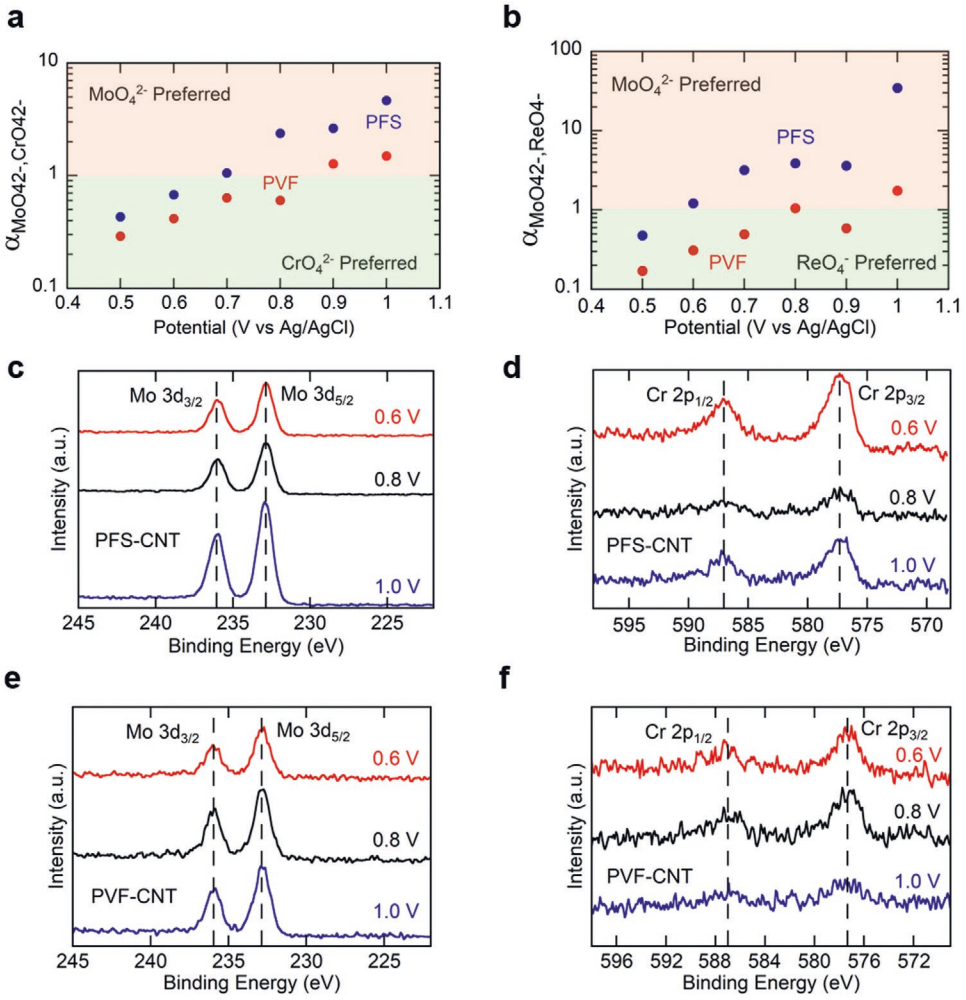

Figure 5. Potential-dependent selectivity. a) Separation factors ($\alpha_{MoO42-,CrO42-}$) measured from electrosorption in 1 mM MoO_4^{2-} and 1 mM CrO_4^{2-} at various potentials. At low potentials, $\alpha_{MoO42-,CrO42-} < 1$, more CrO_4^{2-} is removed than MoO_4^{2-}. At high potentials, $\alpha_{MoO42-,CrO42-} > 1$, more MoO_4^{2-} is removed than CrO_4^{2-}. b) Separation factors ($\alpha_{MoO42-,ReO4-}$) measured from electrosorption in 1 mM MoO_4^{2-} and 1 mM ReO_4^{-} at various potentials. High-resolution c) Mo 3d and d) Cr 2p XPS of PFS-CNT electrodes after electrosorption from 1 mM Na_2MoO_4 and 1 mM Na_2CrO_4 at various potentials. High-resolution e) Mo 3d and f) Cr 2p XPS of PVF-CNT electrodes after electrosorption from 1 mM Na_2MoO_4 and 1 mM Na_2CrO_4 at various potentials.

including ion size, hydrated ion size, and pore size.[32,35] Near-neighbor effects, solvation, and ion-crowding within pores may play a key role in dictating selectivity. Future work using in situ characterization methods will aid in the elucidation of more complex mechanisms for ion selectivity, and shed light into the interplay between structural and potential-dependent selectivity. We believe that potential-dependent selectivity of these polymer electrosorbents introduces a unique approach for controlling ion selectivity, orthogonal from the selectivity that arises from polymer structure—thus allowing for smart, field-controlled strategies for multicomponent ion recovery.

3. Conclusion

Our study has shown that ferrocene-based metallopolymers can selectively capture heavy metal oxyanions, with molecular selectivity modulated by polymer structure and potential. Differential ion selectivity was achieved between PVF, a pendant ferrocene polymer, and PFS, a main-chain ferrocene polymer. Remarkably, PFS was able to deviate from the ion selectivity trend shown by PVF, with PVF-CNT showing selectivity for CrO_4^{2-} over MoO_4^{2-} and ReO_4^{-} over $HAsO_4^{2-}$ while PFS-CNT showed selectivity for MoO_4^{2-} over CrO_4^{2-} and $HAsO_4^{2-}$ over ReO_4^{-} in the binary competitive adsorption tests at 0.8 V versus Ag/AgCl. Quantum mechanical calculations showed that the addition of an electron donating trimethyl–silane group on ferrocene binding sites shifted the binding energy of anions by delocalizing the positive charge away from ferrocene and creating a binding site that included the silane methyl groups. Furthermore, the two ferrocene polymers display potential-dependent selectivity, which creates an additional control parameter for selectivity, distinct from structure selection. Thus, by leveraging both effects derived

from electric potential and chemical structure, we achieve unusual separation factors beyond expected ion-selectivity trends, thus opening new pathways for tailoring interfacial selectivity for advanced energy and environmental applications. In sum, our work presents a promising electrochemically-modulated platform that could significantly advance precision separations, including value-added metal recycling from complex industrial effluents, recovery of critical elements from electronic waste, and even facilitate secondary recovery from mining.

4. Experimental Section

Polyvinylferrocene/Carbon Nanotube and Polyferrocenylsilane/Carbon Nanotube Fabrication: PFS was synthesized via ring opening polymerization of 1,1′-dimethylsilaferrocenophane (full synthesis details in Section S1, Supporting Information). PVF-CNT electrodes were prepared using a dip-coating method.[22] A stock solution "A" containing 80 mg PVF (Polysciences Inc.) and 40 mg multiwalled CNT (Sigma-Aldrich) in 10 mL chloroform and a stock solution "B" of 40 mg multiwalled CNT in 10 mL chloroform were prepared and sonicated for 1 h in icy water. The two stock solutions were mixed in a 1:1 ratio and sonicated again for 1 h in icy water to make solution "A + B". Ti mesh (Fuel Cell Store) was cut into 1.3 cm wide strips and dipped 1 cm deep into "A + B" until the mass of the coating was between 0.65 and 0.9 mg. PFS-CNT electrodes were prepared in a similar way but the PFS "A + B" solution was diluted as 1 part "A + B" with 2 parts chloroform prior to dip coating due to PFS-CNT forming a less stable suspension compared to that of PVF-CNT.

Electrochemical Adsorption and Separation Factor Experiments: Electrochemical techniques were performed using a VersaSTAT 3 potentiostat (Princeton Applied Research). Electrochemical adsorption and separation factor experiments were carried out in a three-electrode cell (BASi) with an Ag/AgCl 3 M NaCl reference (BASi) and a Pt counter using chronoamperometry. All experiments were performed under ambient conditions unless otherwise noted. For adsorption tests, 5 mL of 1 mM sodium oxyanion (Na_2CrO_4, Na_2MoO_4, Na_2HAsO_4, Na_2SeO_4, $NaVO_3$, or $NaReO_4$) with 20 mM $NaClO_4$ was used and the solution was bubbled with N_2 for 1 min prior to submerging the electrode. For kinetic tests, 5 or 6 mL (depending on the test) initial volume was used and 0.1 mL aliquots were taken at different times for ICP assay. An Agilent 5110 ICP-OES instrument was used to quantify concentrations of chromium, molybdenum, arsenic, selenium, vanadium, and rhenium. Aliquots taken from adsorption experiments were diluted in 2% w/w HNO_3 (Fisher Chemical) and assayed against standards made with Cr, Mo, As, Se, V, and Re ICP standards (Sigma-Aldrich). Uptake was calculated using the following equation:

$$\text{Uptake} = \frac{C_0 - C}{m_{\text{polymer}}} V \tag{2}$$

where C_0 was the initial mass basis concentration of the analyte (Cr, Mo, As, Se, V, or Re), C was the mass basis concentration of the analyte during or after adsorption, V was the volume of solution in the cell, and m_{polymer} was the mass of PVF or PFS on the working electrode.

For separation factor tests, 5 mL of solution was used. The solutions contained 1 mM of two sodium oxyanion salts (e.g. 1 mM Na_2CrO_4 and Na_2MoO_4) and were bubbled with N_2 for 1 min. Electrosorption was induced using chronoamperometry. The solution was sampled after 1 h to ensure that equilibrium adsorption had been reached. Samples were assayed the same way as with the previous adsorption tests. Separation factors were calculated using the following equation:

$$\alpha_{A,B} = \frac{N_{A,\text{ads}} / N_{B,\text{ads}}}{N_{A,\text{sol}} / N_{B,\text{sol}}} \tag{3}$$

where $N_{A,\text{ads}}$ and $N_{B,\text{ads}}$ were the molar quantities of oxyanions A and B adsorbed and $N_{A,\text{sol}}$ and $N_{B,\text{sol}}$ were the molar quantities of oxyanions in solution at equilibrium adsorption.

Experiments in the spiked wastewater from Urbana-Champaign Sanity District were performed in a 3D printed 1 mL volume cell without N_2 bubbling.

Materials Characterization: SEM and XPS were carried out in the Frederick Seitz Materials Research Laboratory Central Research Facilities, University of Illinois. SEM was carried out using a Hitachi S-4700 and EDS was carried out with an attached iXRF EDS Elemental Analysis System with Oxford Instruments (Si(Li) detector). XPS was performed using a Kratos Axis ULTRA with a monochromatic Al Ka X-ray source (210 W).

Density-Functional Theory calculations: ORCA 4.0.1.2 was used to perform all density-functional theory (DFT) calculations.[36] The valence triple-zeta quality def2-TZVP basis set[37] and the B3LYP functional[38] were employed at all atoms for both geometry optimization and frequency analysis. All calculations were sped up through the RIJCOSX approximation[39] and were carried out in water solution environment to mimic the physically relevant conditions. The solvation effects were computed by the conductor-like polarizable continuum model using a static dielectric constant of water $\varepsilon = 80.4$ and the refractive index $n = 1.33$. The dispersion effects were included by the DFT-D3 approach with Becke–Johnson damping.[40] The convergence criteria for the maximum norm of the geometry gradient and electronic energy was 10^{-4} hartree/bohr and 10^{-8} hartree (ORCA keywords: TightOpt and TightSCF). To obtain the optimal anion-monomer binding positions, the authors explored different initial coordinates, and then optimized them without any symmetry restrictions. The absence of imaginary frequency verified that final structures were true minima at the current level of theory.

After the geometry optimization, thermal corrections to the Gibbs free energy were estimated at 298.15 K and 1 atm with solvent effect. The thermal corrections include zero-point vibrational energy (ZPE), entropy, and enthalpy contributions. The final Gibbs free energy was calculated from the numerical frequency analysis implemented in ORCA. The binding energy was the difference in the Gibbs free energy between the anion, monomer, and anion-monomer complex:

$$\Delta G = G(\text{monomer}) + G(\text{anion}) - G(\text{complex}) \tag{4}$$

where ΔG represented the binding energy and G corresponded to the total Gibbs free energy. The authors optimized the structures for all three species and then calculated the binding free energy. Charge transferred (Q_{Transfer}) from the anion was calculated by taking the difference between the sum of charges on the anion in the optimized anion-monomer complex and the initial charge of the anion:

$$Q_{\text{Transfer}} = Q_{\text{anion in complex}} - Q_{\text{anion}} \tag{5}$$

Supporting Information

Supporting Information is available from the Wiley Online Library or from the author.

Acknowledgements

This material is based upon work supported by the U.S. Department of Energy, Office of Basic Energy Sciences under Award Number DOE DE-SC0021409 to X.S. and R.C. also thank the University of Illinois Urbana-Champaign and the School of Chemical Sciences for their support through startup funds. X.S. and J.J. also acknowledge partial support by NSF CBET grant 1942971. D.S. acknowledges support from the New Innovator Award in Food & Agriculture Research from Foundation for Food & Agriculture Research. J.F. and D.S. thank the Blue Waters sustained-petascale computing project, which was supported by the National

Science Foundation (Awards OCI-0725070 and ACI-1238993) and the state of Illinois. SEM and XPS were carried out in the Frederick Seitz Materials Research Laboratory Central Research Facilities, University of Illinois. M.G. and C.R. acknowledge the German Research Foundation within the project GA-2169/5-1 for partial financial support of this work. The authors thank Stephen Cotty for his help with making schematics for the figures.

Conflict of Interest

The authors declare no conflict of interest.

Data Availability Statement

The data that support the findings of this study are available from the corresponding author upon reasonable request.

Keywords

electrochemical separations, electrosorption, metal recovery, metallopolymers, redox electrochemistry, water purification, water treatment

Received: October 31, 2020
Revised: December 20, 2020
Published online:

[1] a) M. A. C. Stuart, W. T. S. Huck, J. Genzer, M. Müller, C. Ober, M. Stamm, G. B. Sukhorukov, I. Szleifer, V. V. Tsukruk, M. Urban, F. Winnik, S. Zauscher, I. Luzinov, S. Minko, *Nat. Mater.* **2010**, *9*, 101; b) A. Klaikherd, C. Nagamani, S. Thayumanavan, *J. Am. Chem. Soc.* **2009**, *131*, 4830.

[2] a) X. Su, A. Kushima, C. Halliday, J. Zhou, J. Li, T. A. Hatton, *Nat. Commun.* **2018**, *9*, 4701; b) P. Srimuk, X. Su, J. Yoon, D. Aurbach, V. Presser, *Nat. Rev. Mater.* **2020**, *5*, 517; c) R. Candeago, K. Kim, H. Vapnik, S. Cotty, M. Aubin, S. Berensmeier, A. Kushima, X. Su, *ACS Appl. Mater. Interfaces* **2020**, *12*, 49713; d) K. Kim, P. B. Medina, J. Elbert, E. Kayiwa, R. D. Cusick, Y. Men, X. Su, *Adv. Funct. Mater.* **2020**, *30*, 2004635.

[3] a) M. Arca, M. V. Mirkin, A. J. Bard, *J. Phys. Chem.* **1995**, *99*, 5040; b) A. R. Hillman, *J. Electrochem. Soc.* **1992**, *139*, 74; c) M. W. Espenscheid, C. R. Martin, *J. Electroanal. Chem. Interfacial Electrochem.* **1985**, *188*, 73; d) S. Cosnier, C. Innocent, J. C. Moutet, F. Tennah, *J. Electroanal. Chem.* **1994**, *375*, 233.

[4] a) R. M. Izatt, S. R. Izatt, R. L. Bruening, N. E. Izatt, B. A. Moyer, *Chem. Soc. Rev.* **2014**, *43*, 2451; b) D. S. Sholl, R. P. Lively, *Nature* **2016**, *532*, 435; c) *A Research Agenda for Transforming Separation Science*, National Academies Press, Washington, DC, USA **2019**, http://nap.edu/25421; d) X. Su, *Electrochem. Soc. Interface* **2020**, *29*, 55; e) D. Bauer, D. Diamond, J. Li, M. McKittrick, D. Sandalow, P. Telleen, *Critical Materials Strategy*, US Department of Energy, **2011**, https://www.energy.gov/node/349057.

[5] a) W. Jin, Y. Zhang, *ACS Sustainable Chem. Eng.* **2020**, *8*, 4693; b) H. Wang, Z. J. Ren, *Water Res.* **2014**, *66*, 219.

[6] a) I. Ali, *Chem. Rev.* **2012**, *112*, 5073; b) S. Bolisetty, M. Peydayesh, R. Mezzenga, *Chem. Soc. Rev.* **2019**, *48*, 463; c) Y. Peng, H. Huang, Y. Zhang, C. Kang, S. Chen, L. Song, D. Liu, C. Zhong, *Nat. Commun.* **2018**, *9*, 187.

[7] S. Lata, P. K. Singh, S. R. Samadder, *Int. J. Environ. Sci. Technol.* **2015**, *12*, 1461.

[8] a) C. Liu, P.-C. Hsu, J. Xie, J. Zhao, T. Wu, H. Wang, W. Liu, J. Zhang, S. Chu, Y. Cui, *Nat. Energy* **2017**, *2*, 17007; b) M. Gallei, C. Rüttiger, *Chem. - Eur. J.* **2018**, *24*, 10006.

[9] X. Su, K.-J. Tan, J. Elbert, C. Rüttiger, M. Gallei, T. F. Jamison, T. A. Hatton, *Energy Environ. Sci.* **2017**, *10*, 1272.

[10] a) I. Jureviciute, S. Bruckenstein, A. R. Hillman, *J. Electroanal. Chem.* **2000**, *488*, 73; b) C. Barbero, M. C. Miras, E. J. Calvo, R. Kötz, O. Haas, *Langmuir* **2002**, *18*, 2756.

[11] a) M. Gallei, *Macromol. Chem. Phys.* **2014**, *215*, 699; b) J. Elbert, F. Krohm, C. Rüttiger, S. Kienle, H. Didzoleit, B. N. Balzer, T. Hugel, B. Stühn, M. Gallei, A. Brunsen, *Adv. Funct. Mater.* **2014**, *24*, 1591.

[12] R. L. N. Hailes, A. M. Oliver, J. Gwyther, G. R. Whittell, I. Manners, *Chem. Soc. Rev.* **2016**, *45*, 5358.

[13] a) J. B. Gilroy, T. Gädt, G. R. Whittell, L. Chabanne, J. M. Mitchels, R. M. Richardson, M. A. Winnik, I. Manners, *Nat. Chem.* **2010**, *2*, 566; b) X. He, M.-S. Hsiao, C. E. Boott, R. L. Harniman, A. Nazemi, X. Li, M. A. Winnik, I. Manners, *Nat. Mater.* **2017**, *16*, 481; c) X. Wang, G. Guerin, H. Wang, Y. Wang, I. Manners, M. A. Winnik, *Science* **2007**, *317*, 644; d) T. Gädt, N. S. Ieong, G. Cambridge, M. A. Winnik, I. Manners, *Nat. Mater.* **2009**, *8*, 144; e) J.-C. Eloi, D. A. Rider, G. Cambridge, G. R. Whittell, M. A. Winnik, I. Manners, *J. Am. Chem. Soc.* **2011**, *133*, 8903.

[14] R. Singh, S. Singh, P. Parihar, V. P. Singh, S. M. Prasad, *Ecotoxicol. Environ. Saf.* **2015**, *112*, 247.

[15] Mineral Commodity Summaries, U.S. Geological Survey **2020**, https://pubs.er.usgs.gov/publication/mcs2020.

[16] A. D. Dayan, A. J. Paine, *Hum. Exp. Toxicol.* **2001**, *20*, 439.

[17] J. K. MacFarquhar, D. L. Broussard, P. Melstrom, R. Hutchinson, A. Wolkin, C. Martin, R. F. Burk, J. R. Dunn, A. L. Green, R. Hammond, W. Schaffner, T. F. Jones, *Arch. Intern. Med.* **2010**, *170*, 256.

[18] E. Kim, M. F. Benedetti, J. Boulègue, *Water Res.* **2004**, *38*, 448.

[19] L. Liang, B. Gu, X. Yin, *Sep. Technol.* **1996**, *6*, 111.

[20] J. L. Domingo, *Reprod. Toxicol.* **1996**, *10*, 175.

[21] K. Lourenssen, J. Williams, F. Ahmadpour, R. Clemmer, S. Tasnim, *J. Energy Storage* **2019**, *25*, 100844.

[22] X. Su, J. Hübner, M. J. Kauke, L. Dalbosco, J. Thomas, C. C. Gonzalez, E. Zhu, M. Franzreb, T. F. Jamison, T. A. Hatton, *Chem. Mater.* **2017**, *29*, 5702.

[23] R. Chen, T. Sheehan, J. L. Ng, M. Brucks, X. Su, *Environ. Sci.: Water Res. Technol.* **2020**, *6*, 258.

[24] C. M. Woodbridge, D. L. Pugmire, R. C. Johnson, N. M. Boag, M. A. Langell, *J. Phys. Chem. B* **2000**, *104*, 3085.

[25] a) A. B. Fischer, M. S. Wrighton, M. Umana, R. W. Murray, *J. Am. Chem. Soc.* **1979**, *101*, 3442; b) C. Rüttiger, S. Mehlhase, S. Vowinkel, G. Cherkashinin, N. Liu, C. Dietz, R. W. Stark, M. Biesalski, M. Gallei, *Polymer* **2016**, *98*, 429.

[26] Z. Song, S. Garg, J. Ma, T. D. Waite, *Environ. Sci. Technol.* **2020**, *54*, 12081.

[27] G. Masson, P. Beyer, P. W. Cyr, A. J. Lough, I. Manners, *Macromolecules* **2006**, *39*, 3720.

[28] D. P. Mohapatra, D. M. Kirpalani, *Water Sci. Technol.* **2019**, *79*, 842.

[29] C. M. Hill, *Review of Available Technologies for the Removal of Selenium from Water*, CH2M HILL **2010**, https://www.namc.org/docs/00180231.pdf.

[30] a) K. F. Hayes, A. L. Roe, G. E. Brown, K. O. Hodgson, J. O. Leckie, G. A. Parks, *Science* **1987**, *238*, 783; b) D. Peak, D. L. Sparks, *Environ. Sci. Technol.* **2002**, *36*, 1460; c) L. Zhu, L. Zhang, J. Li, D. Zhang, L. Chen, D. Sheng, S. Yang, C. Xiao, J. Wang, Z. Chai, T. E. Albrecht-Schmitt, S. Wang, *Environ. Sci. Technol.* **2017**, *51*, 8606.

[31] a) R. Amin, M. Edraki, D. Doley, C. Sheridan, *Sci. Total Environ.* **2018**, *637–638*, 1252; b) F. Frascoli, K. A. Hudson-Edwards, *Minerals* **2018**, *8*, 42.

[32] a) C.-H. Hou, P. Taboada-Serrano, S. Yiacoumi, C. Tsouris, *J. Chem. Phys.* **2008**, *129*, 224703; b) L. Yang, S. Garde, *J. Chem. Phys.* **2007**, *126*, 084706.
[33] A. S. J. Wéry, J. M. Gutiérrez-Zorrilla, A. Luque, M. Ugalde, P. Román, *Chem. Mater.* **1996**, *8*, 408.
[34] a) W. Swartz, D. M. Hercules, *Anal. Chem.* **1971**, *43*, 1774; b) M. C. Biesinger, B. P. Payne, A. P. Grosvenor, L. W. M. Lau, A. R. Gerson, R. S. C. Smart, *Appl. Surf. Sci.* **2011**, *257*, 2717.
[35] P. Srimuk, J. Lee, S. Fleischmann, M. Aslan, C. Kim, V. Presser, *ChemSusChem* **2018**, *11*, 2091.
[36] F. Neese, *Wiley Interdiscip. Rev.: Comput. Mol. Sci.* **2018**, *8*, e1327.
[37] F. Weigend, R. Ahlrichs, *Phys. Chem. Chem. Phys.* **2005**, *7*, 3297.
[38] a) A. D. Becke, *J. Chem. Phys.* **1993**, *98*, 5648; b) P. J. Stephens, F. J. Devlin, C. F. Chabalowski, M. J. Frisch, *J. Phys. Chem.* **1994**, *98*, 11623.
[39] F. Neese, *J. Comput. Chem.* **2003**, *24*, 1740.
[40] a) S. Grimme, S. Ehrlich, L. Goerigk, *J. Comput. Chem.* **2011**, *32*, 1456; b) S. Grimme, J. Antony, S. Ehrlich, H. Krieg, *J. Chem. Phys.* **2010**, *132*, 154104.